www.icgst.com

ICGST International Journal on Graphics, Vision and Image Processing (GVIP)

ICGST Original Manuscripts

ICGST – SN: P1150535004
ISSN: 1687-398X Print, 1687-3998 Online, 1687-4005 CD-ROM
Title: "Novel Schemes of Trivariate Linear and One-Dimensional Quadratic B-Spline Interpolation Functions Based on the Sub-pixel Efficacy Region"
Publishing Date: November 2005, Volume (5), Issue (8), Pages (43--53)
Authors: C. Ciulla and F.P. Deek
Address: College of Science and Liberal Arts, New Jersey Institute of Technology
323 M.L.King Blvd. University Heights - Newark, NJ 07102-1982, USA
E-mail: [cxc2728, Fadi.Deek]@NJIT.EDU
URL: http://www.njit.edu

GVIP Journal, Volume 5, Issue 8, August 2005

www.icgst.com

Novel Schemes of Trivariate Linear and One-Dimensional Quadratic B-Spline Interpolation Functions Based on the Sub-pixel Efficacy Region

C. Ciulla * and F.P. Deek [1]

[1] *College of Science and Liberal Arts, New Jersey Institute of Technology*
323 M.L.King Blvd. University Heights - Newark, NJ 07102-1982, USA
* Corresponding author; [cxc2728, Fadi.Deek]@NJIT.EDU

Abstract

A practical approach for the improvement of the interpolation error is presented and is applied to trivariate linear and one-dimensional quadratic B-Spline interpolation functions. The departing point of this work is that of incorporating the intensity-curvature distribution of the given interpolation function into the mathematical formulation named Intensity-Curvature Functional (ΔE). While the intensity is determined by the sequel of discrete samples and also by the values established through interpolation, the curvature is expressed by the sum of second order partial derivatives of the interpolation function. The study continues by finding the solution of the polynomial consisting of the partial derivatives of ΔE with respect to each of the dimensional variables. Such a solution reveals a spatial domain of intra-pixel points called Sub-pixel Efficacy Region (SRE), which is used to improve the approximation characteristics of the interpolator. Thus, for a given re-sampling location and also for given intensity values at the pixel to re-sample and the neighbourhood, the Sub-pixel Efficacy Region is used to determine a novel re-sampling location to calculate the interpolation function. For a signal or an image, the novel re-sampling location varies pixel by pixel depending on (i) the local distribution of pixel intensity across the neighbourhood and (ii) the local curvature of the interpolation function. Benefits and limitations of the application of the SRE are studied in space domain by analysis of root mean square errors, and in frequency domain by analysis of spectral power distributions. Novel schemes of trivariate linear and one-dimensional quadratic B-Spline functions are determined with improved approximation capabilities.

Keywords: *Intensity-Curvature Functional, Sub-pixel Efficacy Region, Novel Re-sampling Location.*

1. Introduction

Recent applications of linear interpolation includes object-based interpolation, which has been initiated in [1], evaluated and extended in [2], and recently reinforced in [3, 4]. This work shows that to linearly interpolate a surface representing the distance map of the pixels from the boundary of the object in the scene proves superior to simply linearly interpolate the pixel intensities. Also a statistical comparison of the shape-based interpolation method was reported in [4]. Such comparison was made within the three-dimensional context against a host of other methods including the classic trivariate linear interpolation, and consistently with what was earlier reported in [5], showed that the object-based method could be useful to reduce both approximation error and smoothing that are inherent to linear interpolation. A more recent example of object-based registration method [6] puts the emphasis on the capability to derive a non-rigid distribution of re-sampling locations to be used by linear interpolation, and demonstrates its superiority with respect to the shape-based interpolation method reported in [3], but nonetheless admits to be computationally expensive.

The issue of determining a framework for the analysis and design of interpolation functions was addressed with the objective of conceptualization of two-dimensional polynomial interpolators as convolution operators, which decompose rotation into a couple of translations along the major axis. Such framework, whose feasibility was demonstrated, embraces a large number of interpolators [7]. Another example of the development of a framework for designing polynomial interpolation functions takes on a diverse form with respect to the more traditional [8]. In this framework the polynomial is composed by the B-Spline with their derivatives [9]. Such interpolators are attributed the characteristic of Minimal Order Minimal Support (MOMS) because they minimize the computational complexity, as related to the degree, and at the same time they offer a trade-off with their interval of definition. Also, their performance was compared to the traditional B-Splines [10]. As it is commonly recognized in the literature, approximation properties of interpolation schemes are strictly dependent on the sampling resolution [9, 11-13]. Also, connecting to the recent trend of local optimization [14, 15] versus global optimization, that is pixel-by-pixel optimization, multi-dimensional B-Spline models were developed in

order to obtain a novel grid of knots as derived from the original grid placement. This is determined by minimizing error bounds that are dependent on derivatives of the interpolation function and that incorporate, at least partially, the function curvature information content [16].

The relevance of this paper is the development of a theory for the improvement of the interpolation error from which a methodology is derived that determines optimal choice of the space domain points where the interpolator is calculated. To accomplish this goal, this work captures the effect of the interpolator on the image pixel intensity by merging together as single parameter: (i) the pixel intensity value and (ii) the curvature of the interpolator as expressed by the sum of its second order partial derivatives. This work also proposes to calculate this single parameter in its distribution across the pixel. The joint information content is thus calculated for each pixel in two terms: (i) at the grid node and (ii) at the generic intra-pixel location. The ratio between the two terms determines the mathematical formulation called Intensity-Curvature Functional (ΔE). Study of ΔE leads to the determination of the spatial domain of points called the Sub-pixel Efficacy Region (SRE). In order to improve the approximation properties of the interpolation function, given an original grid of points and a given re-sampling location, re-sampling takes place at a novel location that varies node by node. Such novel re-sampling location is not necessarily the same as the given re-sampling location and it is determined through the use of the SRE. Thus, the theory yields two conceptions of relevance. The first is the improvement of the interpolation error, determined as dependent on image pixel intensity and curvature of the interpolation function, and the second is re-sampling determined locally rather than globally, that is pixel-by-pixel.

The literature lacks of a unifying framework that achieves error improvement regardless of the dimensionality or degree of the interpolation function. The theory proposed here is applied to trivariate liner and one-dimensional quadratic B-Spline functions. Nevertheless, this paper also presents results of the application of the theory to the bivariate linear and the cubic Lagrange functions and thus proposes a framework that is based on the Sub-pixel Efficacy Region and that is unifying in its purpose. The framework determines interpolation error improvement as dependent on the joint information content of pixel intensity and curvature of the interpolation function, and it does that, regardless of the dimensionality and the degree of the interpolator.

The rest of the paper is organized as follows. The next section presents the theory. This is followed by the results section where a validation paradigm, based on motion correction, is used to study the behaviour of the root mean square error (RMSE) and to show the interpolation error improvement. Also, Fast Fourier Transforms and spectra power analyzers are employed to study the effect in the frequency domain of the Sub-pixel Efficacy Region on the interpolated images. Finally the result of this work and its implication is discussed within the context of the current literature.

2. Theory

In practical applications, given a discrete sample of intensity values, the interpolation function, attempts to reconstruct a continuous signal from it. In order to truly discriminate the value of the function at a particular sampling point it is necessary, based on the samples, to have information about concavity and convexity of the function itself. Even if two values determined by the interpolation function are numerically the same, there might exist a difference between them that goes beyond the value itself. This happens because of the local convexity or concavity of the function. To determine the difference between the two values, there is thus a need to calculate the joint information content of the value furnished by interpolation, which is represented by the image pixel intensity, and the curvature of function. This joint information content will be calculated for each pixel in two intensity-curvature terms: (i) at the grid node and will be named Eo and (ii) at the generic intra-pixel location and will be named E_{IN}. The discriminative information content that is relevant to the behaviour of the function is therefore increased as opposed to considering the intensity values alone. Two terms are calculated because they are needed to discriminate between the intensity-curvature content determined when the re-sampling point is coincidental with the original grid point, which is the same as not re-sampling, and when the re-sampling point is anywhere in the pixel. The two intensity-curvature terms thus differentiate the condition of re-sampling versus the absence of re-sampling. Their ratio is called the Intensity-Curvature Functional ΔE and it is a measure of the effect of the interpolation function on the image pixel, and since each of the two terms Eo and E_{IN} is calculated by integration, ΔE also measures the intensity-curvature distribution of the interpolation function across the pixel.

The numerical solution of the polynomial system, determined by the first order partial derivative of ΔE with respect to each of the dimensional variables of the interpolation function, will determine the so called Sub-pixel Efficacy Region (SRE). The Sub-pixel Efficacy Region is thus a spatial set of intra-pixel points. The need for the SRE is that of an intra-pixel reference point that can be used to project a given re-sampling location m into a novel re-sampling location m^r where the curvature of the interpolation function assumes approximation characteristics that allow to improve the interpolation error. Both the SRE and its derived novel re-sampling location vary pixel-by-pixel across the discrete sample which constitutes the image. This happens, as it will be seen from the formulation of ΔE, because of their dependency on the relationship existing between image pixel intensities at the neighbourhood and the local curvature of the interpolation function. Thus, the overall aim of the theory is that of reducing the interpolation error by finding the novel re-sampling location where to calculate the interpolator with improved approximation characteristics. This is accomplished here under the umbrella of a unifying framework that works regardless of the dimensionality and the degree of the interpolation function.

2.1 Trivariate Linear

Let h = h(x, y, z) be the trivariate linear interpolation function. Let's assume its continuity across its interval of definition and so for its derivatives. Let it be in the form:

$$h(x, y, z) = f(0,0,0) + x\,\theta_x + y\,\theta_y + z\,\theta_z + xy\,\theta_{xy} + xz\,\theta_{xz} + yz\,\theta_{yz} + xyz\,\omega_f \quad (1)$$

$$\theta_x = f(1,0,0) - f(0,0,0),$$

$$\theta_y = f(0,1,0) - f(0,0,0),$$

$$\theta_z = f(0,0,1) - f(0,0,0),$$

$$\theta_{xy} = (f(0,0,0) - f(1,0,0) - f(0,1,0) + f(1,1,0)),$$

$$\theta_{xz} = (f(0,0,0) - f(1,0,0) - f(0,0,1) + f(1,0,1)),$$

$$\theta_{yz} = (f(0,0,0) - f(0,1,0) - f(0,0,1) + f(0,1,1)),$$

$$\omega_f = (f(1,1,1) - f(1,1,0) - f(0,1,1) - f(1,0,1) + f(0,0,1) + f(0,1,0) + f(1,0,0) - f(0,0,0))$$

Where f(0,0,0), f(1,0,0), f(1,1,0), f(0,1,0) and f(0,0,1), f(1,0,1), f(1,1,1), f(0,1,1) are the two quadruple of values at the vertices the three dimensional pixel. For the trivariate liner interpolation function h(x, y, z), let the curvature Ω(x, y, z) be represented by the sum of the three second order partial derivatives:

$$\Omega(x, y, z) = \left(\frac{\partial^2 h(x, y, z)}{\partial x \partial y} + \frac{\partial^2 h(x, y, z)}{\partial x \partial z} + \frac{\partial^2 h(x, y, z)}{\partial y \partial z} \right)$$

The two intensity-curvature terms are calculated as:

$$E_0(x, y, z) = \int_0^x \int_0^y \int_0^z f(0, 0, 0)\, \Omega_0(x, y, z)\, dx\, dy\, dz \quad (2)$$

$$E_{IN}(x, y, z) = \int_0^x \int_0^y \int_0^z h(x, y, z)\, \Omega(x, y, z)\, dx\, dy\, dz \quad (3)$$

Where $\Omega_0(x, y, z) = \Omega(0, 0, 0)$. The Intensity-Curvature Functional results in:

$$\Delta E = \Delta E(x, y, z) = \frac{E_0(x, y, z)}{E_{IN}(x, y, z)} = \frac{x\, y\, z\, f(0, 0, 0)\, (\theta_{xy} + \theta_{xz} + \theta_{yz})}{[(\theta_{xy} + \theta_{xz} + \theta_{yz}) + \omega_f\, (x + y + z - 3)]\, H_{xyz}(x, y, z)} \quad (4)$$

$H_{xyz}(x, y, z)$ is the primitive function of h(x, y, z) with respect to x, y and z. Also, θ_{xy}, θ_{xz}, θ_{yz} and ω_f express relationships between f(0, 0, 0), which is the intensity at the pixel to re-sample and the pixel intensity values at its neighbourhood. The Sub-pixel Efficacy Region is defined as:

$$\Phi = \left\{ (x, y, z) : \left(\frac{\partial \Delta E}{\partial x} \right) = 0, \left(\frac{\partial \Delta E}{\partial y} \right) = 0, \left(\frac{\partial \Delta E}{\partial z} \right) = 0 \right\} \quad (5)$$

Where the number of SRE points $(x_{sre}, y_{sre}, z_{sre}) = (x, y, z) \in \Phi$ is coincidental with the degree of the polynomial system resulting from the three derivatives of ΔE with respect to x, y, and z. Solution of (5) furnishes:

$$x_{sre}^{(1)} = \frac{2\sqrt{f(0,0,0)^2 - 1}}{\lambda_{x1}}; \; x_{sre}^{(2)} = \frac{-2\sqrt{f(0,0,0)^2 - 1}}{\lambda_{x2}};$$

$$y_{sre}^{(1)} = \frac{2\left(-f(0,0,0) + \sqrt{f(0,0,0)^2 - 1} \right)}{\theta_y};$$

$$y_{sre}^{(2)} = \frac{-2\left(f(0,0,0) + \sqrt{f(0,0,0)^2 - 1} \right)}{\theta_y};$$

$$z_{sre}^{(1)} = \frac{2\sqrt{f(0,0,0)^2 - 1}}{\lambda_{z1}}; \; z_{sre}^{(2)} = \frac{-2\sqrt{f(0,0,0)^2 - 1}}{\lambda_{z2}};$$

Where:

$$\lambda_{x1} = \frac{\theta_{xy}\, \omega_f \left(-f(0,0,0) + \sqrt{f(0,0,0)^2 - 1} \right)}{\theta_y} - \theta_x;$$

$$\lambda_{x2} = \frac{\theta_{xy}\, \omega_f \left(-f(0,0,0) - \sqrt{f(0,0,0)^2 - 1} \right)}{\theta_y} - \theta_x;$$

$$\lambda_{z1} = \frac{\theta_{zy}\, \omega_f \left(-f(0,0,0) + \sqrt{f(0,0,0)^2 - 1} \right)}{\theta_y} - \theta_z;$$

$$\lambda_{z2} = \frac{\theta_{zy}\, \omega_f \left(-f(0,0,0) - \sqrt{f(0,0,0)^2 - 1} \right)}{\theta_y} - \theta_z;$$

$$\frac{h(x_{sre} - x^{r0}, y_{sre} - y^{r0}, z_{sre} - z^{r0})}{h(x_{sre}, y_{sre}, z_{sre})} * \frac{Curv\,(x_{sre} - x^{r0}, y_{sre} - y^{r0}, z_{sre} - z^{r0})}{Curv\,(x_{sre}, y_{sre}, z_{sre})} = \frac{E_{IN}(x_{sre} - x_0, y_{sre} - y_0, z_{sre} - z_0)}{E_{IN}(x_{sre}, y_{sre}, z_{sre})} \quad (6)$$

Given misplacement (x_0, y_0, z_0), in order to improve the interpolation function error, the function is calculated at

the novel re-sampling location (x^{r0}, y^{r0}, z^{r0}), which is obtained from (6), where:

$$\mathrm{Curv}(x_{sre}-x^{r0}, y_{sre}-y^{r0}, z_{sre}-z^{r0}) = \left[\left(\frac{\partial^2 h(x,y,z)}{\partial x \partial y}\right) + \left(\frac{\partial^2 h(x,y,z)}{\partial x \partial z}\right) + \left(\frac{\partial^2 h(x,y,z)}{\partial y \partial z}\right)\right]_{(x_{sre}-x^{r0}, y_{sre}-y^{r0}, z_{sre}-z^{r0})}$$

$$\mathrm{Curv}(x_{sre}, y_{sre}, z_{sre}) = \left[\left(\frac{\partial^2 h(x,y,z)}{\partial x \partial y}\right) + \left(\frac{\partial^2 h(x,y,z)}{\partial x \partial z}\right) + \left(\frac{\partial^2 h(x,y,z)}{\partial y \partial z}\right)\right]_{(x_{sre}, y_{sre}, z_{sre})}$$

2.2 One-dimensional Quadratic B-Spline

The quadratic B-Spline form that is being studied has a neighbourhood of 3 x 2:

$$h(x) = \begin{cases} -2a|x|^2 + \dfrac{(a+1)}{2} & 0 \le |x| \le 1/2 \\ a|x|^2 - \left(2a+\dfrac{1}{2}\right)|x| + \dfrac{3(a+1)}{4} & 1/2 \le |x| \le 3/2 \end{cases} \quad (7)$$

For this function, the curvature is represented by the single second order derivative:

$$\left(\frac{\partial^2 h(x)}{\partial x^2}\right)$$

The two intensity curvature terms are calculated as:

$$Eo(x) = \int_0^x f(0) \left(\frac{\partial^2 h(x)}{\partial x^2}\right)_{(x=0)} dx \quad (8)$$

$$E_{IN}(x) = \int_0^x h(x) \left(\frac{\partial^2 h(x)}{\partial x^2}\right) dx \quad (9)$$

The Intensity-Curvature Functional:

$$\Delta E = \Delta E(x) = \frac{E_0(x)}{E_{IN}(x)}$$

is calculated as:

$$\Delta E(x) = \frac{x\,\theta_{[a,0]}}{|x|^3\,\theta_{a3} + |x|^2\,\theta_{a2} + |x|\,\theta_{a1}} \quad (10)$$

Where the theta values are defined in Table I.

Quadratic B-Spline
$\theta = [\ 2a \mid (f(1/2)+ f(-1/2)+f(-1)+ f(1)+(f(3/2)+ f(-3/2)) \mid]$
$\theta_{[a,0]} = f(0)\ \theta$
$\theta_{[a,1/2]} = [f(1/2)+f(-1/2)]\ \theta$
$\theta_{[a,3/2]} = [(f(1/2)+ f(-1/2)+f(-1)+ f(1)+(f(3/2)+ f(-3/2))]\ \theta$
$\theta_{a1} = \theta_{[a,0]} + ((a+1)/2)\ \theta_{[a,1/2]} + (3(a+1)/4)\ \theta_{[a,3/2]}$
$\theta_{a2} = ((2a+0.5)/2)\ \theta_{[a,3/2]}$
$\theta_{a3} = (a/3)\ \theta_{[a,3/2]} - (2a/3)\ \theta_{[a,1/2]}$

Table I. Theta values for (10)

The Sub-Pixel Efficacy Region is defined as:

$$\Phi = \left\{ x_{sre}^{(i)} = x : \left(\frac{\partial \Delta E}{\partial x}\right) = 0,\ i = 1, 2...k \right\} \quad (11)$$

Where k is the degree of the polynomial obtained equating to zero the first order derivative of the Intensity-Curvature Functional. Solution of (11) furnishes:

$$x_{sre}^{(1)} = \frac{\theta_{p1} + \sqrt{\theta_{p1}^2 + \theta_{p2}}}{\theta_{p3}};\ x_{sre}^{(2)} = \frac{\theta_{p1} - \sqrt{\theta_{p1}^2 + \theta_{p2}}}{\theta_{p3}};$$

Where:

$$\theta_{p1} = \frac{-3\,\theta_{[a,3/2]}(2a+0.5)}{2};\ \theta_{p3} = -4\left(\frac{a\,\theta_{[a,3/2]}}{3} - \frac{2a\,\theta_{[a,1/2]}}{3}\right);$$

$$\theta_{p2} = -4\,\theta_{p3}\left(\theta_{[a,0]} + (a+1)\theta_{[a,1/2]} + \frac{3(a+1)\theta_{[a,3/2]}}{4}\right).$$

Given misplacement x_0, in order to improve the interpolation function error, the function is calculated at novel re-sampling locations x^{r0}, which is derived from the following formula:

$$\frac{h(x_{sre}-x^{r0})}{h(x_{sre})} * \frac{\mathrm{Curv}(x_{sre}-x^{r0})}{\mathrm{Curv}(x_{sre})} = \frac{E_{IN}(x_{sre}-x_0)}{E_{IN}(x_{sre})} \quad (12)$$

Where:

$$\mathrm{Curv}(x_{sre}-x^{r0}) = \left(\frac{\partial^2 h(x)}{\partial x^2}\right)_{(x_{sre}-x^{r0})}$$

$$\mathrm{Curv}(x_{sre}) = \left(\frac{\partial^2 h(x)}{\partial x^2}\right)_{(x_{sre})}$$

3. Results

Values of misplacement are reported throughout the text and figures as pure numbers, with the intent that the behaviour of the root mean square error (RMSE) for varying misplacement is seen as a lookup table for the corresponding values of sampling resolution. In the following, classic interpolation refers to trivariate linear and B-Spline interpolation which formulas are (1) and (7) respectively. SRE-based interpolation refers to the classic interpolation functions calculated at the novel re-sampling location, obtained from (6) and (12) respectively, for the trivariate linear and the B-Spline. With the aim to show the error improvement obtained by the theory, the validation approach based on motion correction was used as follows. A given signal is calculated at an intra-node misplacement *m,* which can either be (x_0, y_0, z_0) for the trivariate linear or x_0 for the B-Spline. The signal was motion corrected and interpolated using *m* and the RMSE was calculated. Also, based on *m*, a novel re-sampling location m^r was obtained, which can either be (x^{r0}, y^{r0}, z^{r0}) calculated from (6) for the trivariate linear, or x^{r0} calculated from (12) for the B-Spline. The novel re-sampling location was used for motion correction and interpolation. The RMSE was calculated in this case as well. In the following, $RMSE^{before}$ and $RMSE^{after}$ indicate the root mean square error obtained with classic interpolation and with SRE-based interpolation respectively. The RMSE ratio of improvement is defined as:

$$R = \left(1 - \frac{RMSE^{before}}{RMSE^{after}}\right)$$

A negative value of R indicates an improvement achieved by the SRE-based interpolation function over the corresponding classic. Like wise, positive values indicate the opposite. In the remainder of the text, and in order to simplify, the term *processed* will be used to indicate that the signal or the image was *motion corrected and interpolated*. Thus when stating that the signal was processed, this implies to the reader that the signal was motion corrected and interpolated.

3.1 Validation Procedure

3.1.1 Real Data

Real data were employed to reveal interpolation error improvement and also to study the spectral characteristics of the processed images. Data consisted of: (i) 128 x 128 "Lena" image sub-sampled from an original size matrix of 208 x 222; (ii) Magnetic Resonance Image (MRI) and functional MRI volumes of the human brain. Axial resolution is 128 x 128 [2.0 x 2.0 mm] for the MRI volume and 64 x 64 [3.75 x 3.75 mm] for the functional MRI volume, with 18 and 16 slices respectively, and 6.00 mm inter-slice resolution for both. The MRI volume was down-sampled from the original matrix size of 256 x 256; and (iii) A 238 x 253 matrix of an MRI sagittal slice. For the MRI and the functional MRI volumes, for each slice an RMSE was calculated and thus $RMSE^{before}$ and $RMSE^{after}$ are cumulative of the sum of all slice's RMSE. As for the validation of the SRE-based trivariate linear interpolation, ten functional MRI volumes with recording parameters described in [17] were used and they were corresponding to eight different subjects.

3.1.2 Spectral Power Analysis

The aim of this investigation is to quantify interpolation improvement in terms of differences in spectral power distribution. The entire range of magnitudes derived from the Fast Fourier Transform (FFT) was divided into 2000 intervals each of which corresponded to a magnitude range of same size. The sum of the square of the magnitudes, that is the spectral energy, was determined in each of the 2000 intervals and therefore what resulted was a spectral power distribution. Its behaviour was analyzed for the original image, the image processed with classic interpolation, and the image processed with SRE-based interpolation. The idea was to capture, in each interval, the difference between the spectral energy of the original image and the spectral energy of the two images processed respectively with classic and SRE-based interpolation, and to determine which spectral energy among the two was more closely matching the spectral energy of the original image. The same approach was used for the trivariate linear function. The attention was focused on the highest energy range, and thus intervals from 970 through 1036 were analyzed in the following manner. For each interval, the absolute value of the difference between the spectral energy derived from the original image (O_E) and the spectral energy derived from the image processed with classic interpolation (NOSRE_E) was calculated. This difference was named *abs(O_E - NOSRE_E)*. Also, for each interval, the absolute value of the difference between the spectral energy derived from the original image (O_E) and the spectral energy derived from the image processed with SRE-based interpolation (SRE_E) was calculated. This difference was named *abs(O_E - SRE_E)*. The difference *abs(O_E - SRE_E) - abs(O_E - NOSRE_E)* was then plotted against each magnitude interval in order to obtain a spectral power analyzer.

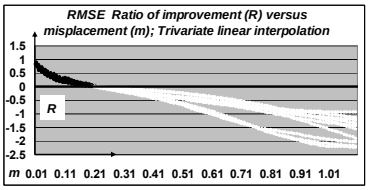

Figure 1. RMSE analysis for the trivariate linear interpolation. Plot of R versus misplacement for ten fMRI volumes. The white portion of the curves indicates interpolation error improvement achieved by SRE.

3.2 Trivariate Linear

Real data experimentation was performed to study the behaviour of the root mean square error in the two conditions of processing the image with classic trivariate interpolation and the corresponding SRE-based paradigm. Figure 1 shows the plot of R for each of the ten functional

MRI volumes for misplacement $(x_0, y_0, z_0) \in [(0, 0, 0), (1.1, 1.1, 1.1)]$ increasing from (0, 0, 0) at simultaneous steps of 0.01 along x, y and z. In the abscissa a value of $(x_0, y_0, z_0) = (0.01, 0.01, 0.01)$ is represented by the value 0.01, and so forth. The portion of the curves in white shows the superiority of the SRE-based interpolation for misplacements that were above $(x_0, y_0, z_0) \equiv (0.2, 0.2, 0.2)$.

3.3 One-dimensional Quadratic B-Spline

Results were collected with real data. Figure 2 shows in (a) the original "Lena" image and in (b) the plot of R. The plot in (b) is versus the values of the parameter "a" $\in$ [-2.34, 2.34] at steps of 0.1. The parameter "a" is indicated in (7). For each of the nine misplacements $x_0 \in$ [0,01, 0.09] at steps of 0.01, an R value was calculated. Thus each R in figure 2b is a sum over nine values. In figure 2c, the plot of R is displayed versus the misplacement $x_0 \in [0, 0.11]$ at steps of 0.001 for "a"=-1.14. Figure 3 shows the plot of R versus misplacement $x_0 \in [0, 0.11]$ at steps of 0.001 ("a"=-1.14) for: the MRI volume (a), the functional MRI volume (b), and the sagittal MRI slice (c). White shows error improvement caused by the SRE, black shows lack of improvement.

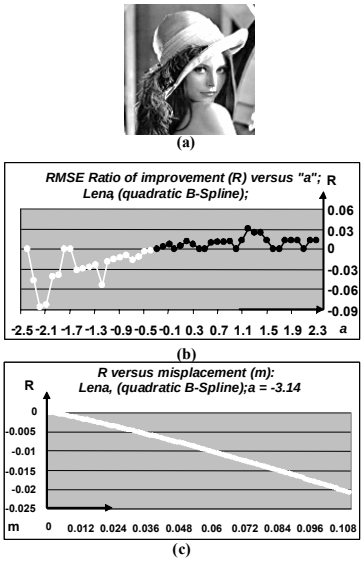

Figure 2. Quadratic B-Spline. (a) Original "Lena" image; (b) plot of R versus "a"; (c) plot of R versus misplacement ("a"=-1.14).

3.4 Power Spectra

Images with the original matrix size were used to calculate the FFT to avoid contamination of results from aliasing effects. There is a corresponding FFT magnitude interval for each interval of the spectral power analyzer and thus a spectral energy. If the difference *abs(O_E - SRE_E) - abs(O_E - NOSRE_E)* is positive, then the spectral energy obtained by processing with classic interpolation was closer to the spectral energy of the original image. Inversely, if the above difference was negative then the spectral energy obtained by processing with SRE-based interpolation was closer to the spectral energy of the original image.

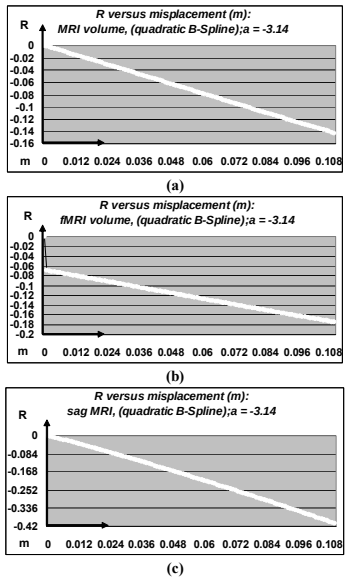

Figure 3. Quadratic B-Spline. Plot of R versus misplacement for: the entire MRI volume of 18 slices (a); the entire functional MRI volume of 16 slices (b); and the sagittal MRI slice (c).

No threshold was applied to the brain images suggesting that the SRE improvement methodology is capable of handling noise as well as signal.

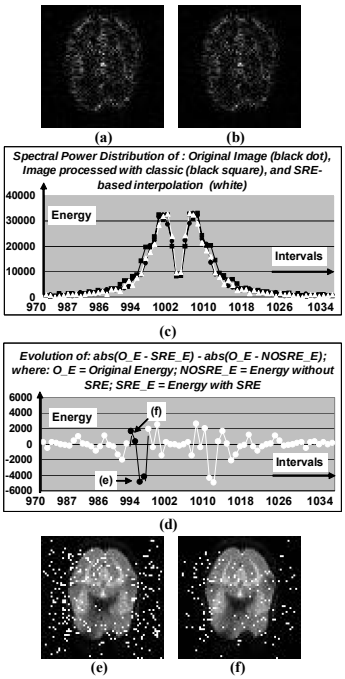

Figure 4. For a functional MRI slice of the volume, and for $(x_0, y_0, z_0) = (0.23, 0.23, 0.23)$. (a) RSE image obtained with classic trivariate linear interpolation; (b) RSE image obtained with SRE-based trivariate interpolation; (c) spectral power distribution; (d) spectral power analyzer; and (e) and (f): White overlay at the pixel locations that correspond to spectral energy indicated by the arrow in (d).

3.4.1 Trivariate Linear

Figure 4 shows the following results: (a) root square error (RSE) image obtained processing with classic trivariate linear interpolation; (b) RSE image obtained processing with SRE-based trivariate interpolation; (c) spectral power distribution; (d) spectral power analyzer. The misplacement was (x_0, y_0, z_0) = (0.23, 0.23, 0.23). Each interval in the spectral power analyzer corresponds to a number of pixels in the image. It was possible to retrieve them and to overlay onto the image. Black dots in figure 4d show values of the difference *abs(O_E - SRE_E) - abs(O_E - NOSRE_E)* which correspond to pixels that are shown in figures 4e and 4f as white overlay onto functional MRI. In figure 4e, shown are those pixels for which the SRE-based trivariate linear interpolation determined spectral energy more closely matching the one of the original image. In figure 4f, shown are those pixels for which the classic trivariate function determined spectral energy more closely matching the one of the original image. For other experimentations performed, the general behaviour observed was that for increasing error improvement, the spectral energy obtained processing the image with SRE-based trivariate linear interpolation was more closely matching that of the original image than the spectral energy obtained processing the image with classic trivariate linear interpolation.

3.4.2 One-dimensional Quadratic B-Spline

For the MRI slice of figure 5a, the FFT histogram is shown in (b). In (c) and (d) of figure 5 are shown respectively the FFT histogram of the image processed with classic quadratic B-Spline as per (7), and the FFT histogram of the image processed with SRE-based quadratic B-Spline. Also, (e) shows the absolute value of the difference between the histograms shown in (b) and (c); (f) shows the absolute value of the difference between the histograms shown in (b) and (d); and finally (g) shows the absolute value of the difference between the histograms shown in (c) and (d). Figures 5e, 5f and 5g demonstrate that the image processed with SRE-based quadratic B-Spline has the FFT histogram that is different from that of the image processed with classic quadratic B-Spline. Similar behavior was observed using "Lena", the sagittal MRI and functional MRI. Thus, to extract the difference between spectra, the analysis was focused on the spectral power distribution and respective spectra power analyzers. In Figure 6, for the functional MRI axial slice shown in (a) and for the sagittal MRI slice shown in (b), a misplacement of x_0 = 0.7 with "a"= -1.14 was used to determine the spectral power analyzers that are shown respectively in (c) and (d).

3.5 Extension of the Theory

This section presents results relative to the improvement of classic bivariate linear and classic cubic Lagrange interpolation functions. The purpose is to demonstrate the flexibility of the approach and the capability of the theory to embrace, under the same unifying approach for the improvement of the interpolation error, interpolators of diverse degrees

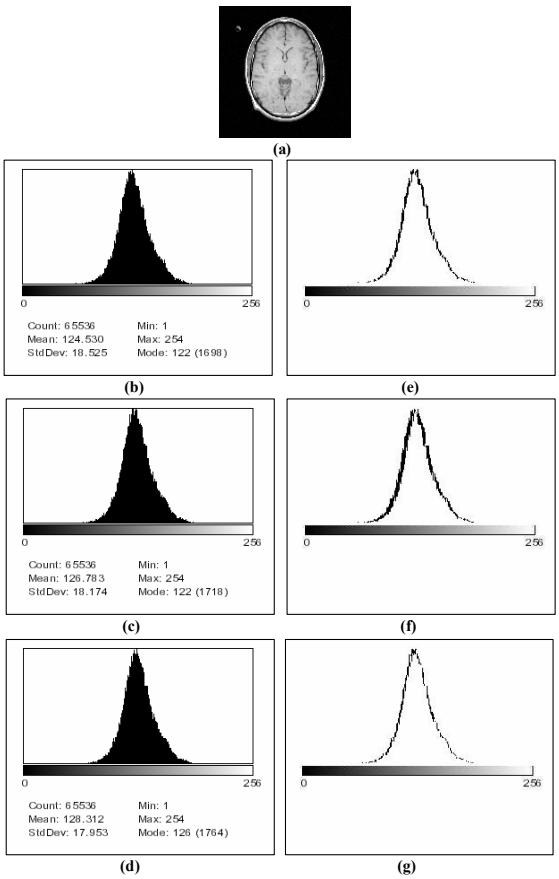

Figure 5. Quadratic B-Spline. For the MRI slice, x_0 = 0.7 and "a"= -1.14. (a) Original image shown as re-sized to a matrix of 128 x 128 and its FFT histogram shown in (b). FFT Histogram for the image processed with classic quadratic B-Spline (c) and quadratic SRE-based B-Spline (d). Respectively in (e), (f) and (g) are shown absolute values of the difference between histograms shown in (b) and (c), (b) and (d), and (c) and (d). The FFT was calculated based on the original matrix resolution of 256 x 256.

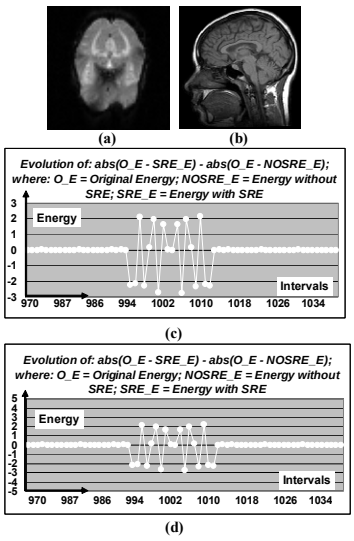

Figure 6. Quadratic B-Spline. (a) Functional MRI axial slice, (b) sagittal MRI slice. Spectral power analyzers obtained processing with classic and SRE-based quadratic B-Spline functions for functional MRI (c), and sagittal MRI (d).

and diverse dimensions. It thus presents evidence that, for these two interpolators, it is possible to derive corresponding SRE-based interpolation functions which allow improved approximation properties over the classic schemes. The classic form of the bivariate linear function used for experimentation is:

$$h(x, y) = f(0,0) + x\,(f(1,0) - f(0,0)) + y\,(f(0,1) - f(0,0)) + xy\,(f(1,1) + f(0,0) - f(0,1) - f(1,0)) \quad (13)$$

where f(0,0), f(1,0), f(0,1) and f(1,1) are the grid values of intensity at the four corners of the pixel. The classic cubic form of the Lagrange interpolation function had the following formulation:

$$h(x) = \begin{cases} (1/2)|x|^3 - |x|^2 - (1/2)|x| + 1 & 0 = |x| = 1 \\ -(1/6)|x|^3 + |x|^2 - (11/6)|x| + 1 & 1 = |x| = 2 \end{cases} \quad (14)$$

And it was calculated with a 2 x 2 neighbourhood of grid nodes' pixel intensity: f(-1), f(1), f(-2), f(2), centred at f(0).

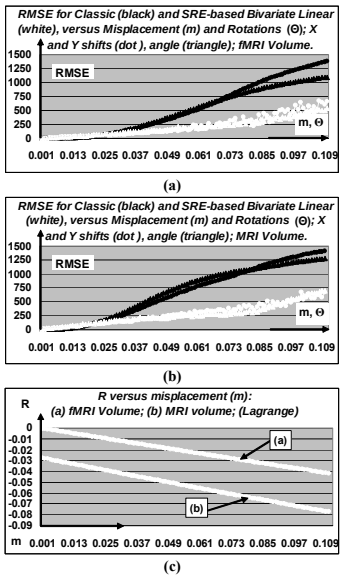

Figure 7. RMSE analysis for classic (black) and SRE-based bivariate linear function (white) for functional MRI (a) and MRI (b) volumes. In (c), shown is the plot of R obtained with classic and SRE-based cubic Lagrange functions with the same set of data.

While the mathematics for the improvement of (13) was reported in [18], it is beyond the scope of the present paper to report the mathematical formulation that permits the improvement of (14). Figures 7a and 7b show the plot of the RMSE for the 16 slices of the functional MRI volume and the 18 slices of the MRI volume, respectively, obtained when processing the data with classic (black) and SRE-based bivariate liner interpolation functions (white). The misplacement was $(x_0, y_0) \in [(0, 0), (0.11, 0.11)]$ and the rotation was $\Theta \in [0, 0.11$ deg] increasing from (0, 0) or 0 deg at steps of 0.001 along x and y, or Θ. In the abscissa a value of $(x_0, y_0) = (0.01, 0.01)$ is represented by the value 0.01, and so forth. Figure 7c shows the evolution of R across the range of one-dimensional misplacements $x_0 \in [0, 0.11]$ cumulated over the 16 slices of the functional MRI volume (curve a), and the 18 slices of the MRI volume (curve b). The improvement in interpolation error shown in figure 7c was obtained processing the data with classic and SRE-based cubic Lagrange interpolation functions. Similarly to what was reported for the quadratic SRE-based B-Spline in [18], experimentation was conducted aiming to investigate the behaviour of the SRE-based Lagrange interpolation function in the estimation of known signals, such to gain knowledge on how the estimation would be in the case of signals unknown at a particular sampling location, and how this estimation would be performed in comparison with the classic form of Lagrange function (14). The signals studied were cos (x) and sin (x). The sampling resolution was 0.01 and the re-sampling location $m_0 \in [0, 0.011]$ increased from 0 at steps of 0.0001 for 111 steps. The value of ratio of improvement R achieved by the SRE-based Lagrange interpolation function is plotted in figure 8 versus the re-sampling location m_0 and indicates improved performance in the estimation of the true value of the signal with respect to the classic paradigm of (14). Similar results were obtained with ln (x) and also with sampling resolutions of 0.1 and 0.001.

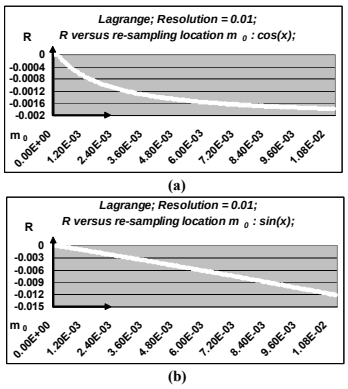

Figure 8. Lagrange ratio of improvement R in estimation of known signals. Estimation at location x^{r0} in place of x_0 for intra-node resolutions of 0.01: (a), (b); respectively for cos (x), sin (x).

4. Discussion and Conclusions

4.1 Characteristics of the Sub-pixel Efficacy Region

The theoretical framework presented in this paper makes use of the Intensity-Curvature Functional (ΔE) expressed as ratio between two intensity-curvature terms of which one is calculated at the grid point and the other at the generic intra-pixel location. One, or more, extremes of ΔE within the sampling step is found and constitutes the intra-pixel space domain of points called Sub-pixel Efficacy Region (SRE). The novel re-sampling locations are obtained based on the SRE. Consequently to the definition of ΔE, it follows that the Sub-pixel Efficacy Region and so the novel re-sampling locations can be different across nodes because of different intensity

values distribution at the neighbourhood and consistently also different curvature of the interpolation function. Thus, within an image, for given motion estimate, re-sampling was considered as an issue having local relevance, based on: (i) the magnitude of misplacement and (ii) the relationships between values of intensity at neighbouring nodes.

4.2 Fourier Properties of the SRE

Study of Fourier properties of interpolators with particular attention to B-Spline functions were reported in [19] and later reinforced in [20] by clearly pointing to the superiority of pass-band properties of B-Splines of degree 2, 4, and 5. Filtering capabilities of B-Splines were studied, that is the capability to derive the B-Spline signal from the B-Spline coefficients [10, 21, 22], or inversely to derive the B-Spline coefficients from the B-Spline signals [23], and it was also reported a generalized formula for the determination of the B-Spline coefficients of the kernel [23]. More generally, it is established in the literature that there exists tight connection between frequency and time domain properties of the interpolation functions [19, 20]. The data presented here, viewed within the context of the frequency domain, show that the Sub-pixel Efficacy Region interpolation improvement approach provides to the interpolator capabilities to change the band-pass filtering. Also, results of this research confirm the capability of SRE, which is inherent to the property of pixel-by-pixel re-sampling, to incorporate frequencies that are discarded by classic interpolation.

4.3 The Resulting Framework

Frameworks that group together different classes of interpolators are reported in literature and give foundations to B-Splines [24], provide a complete description of polynomial interpolation [8], and report extensive mathematical description of B-Splines [22] and their application in signal processing [10, 22]. More recent work aims to derive a unifying formulation of parametric piecewise polynomial interpolation [25] and also to characterize B-Spline digital filters [23].

To place the framework resulting from the present research in the context of current literature, it is important to emphasize that the theory proposed here presents aspects of setting interpolation error dependent on pixel intensity and the curvature of the interpolation function. This differentiates the present work with respect to the various forms of error characterization that are reported in literature [11-13, 26]. To establish originality, the first step was that of embedding the combined information content of function value and curvature into the Intensity-Curvature Functional, as per (4) and (10), respectively, for the trivariate linear and the quadratic B-Spline. The second step was that of using (6) and (12) to compute the novel re-sampling location which leads to improved approximation characteristics, for trivariate linear and B-Spline interpolation respectively. The framework is thus consisting of (4), (10), and (6), (12) and allows variable re-sampling locally, that is changing its location pixel-by-pixel. This property is brought to the SRE-based interpolation functions by the relationships that are used to calculate the novel re-sampling locations. It is also important to admit however that in some cases the approach proposed by the theory does not achieve interpolation error improvement or improve the band-pass characteristics of the interpolator. This might be consequential to the unifying challenge of the mathematical formulation herein proposed and it results in being a limitation of the theoretical framework.

4.4 The Bridging Concept of the Unifying Theory

Interpolation schemes were first introduced based on finite differences [26], and later developed their approximation properties based on the pixel-signal intensity [8, 9, 12, 13, 21, 22, 24, 27, 28], and diversified also into scene-based interpolation paradigms based on pre-processing that extracts significant information from the object in the image [1-4]. The novel class of interpolators introduced by this work, specifically the SRE-based functions, distinguish themselves from the above two main typologies because of the capability to develop approximation properties based on intensity-curvature information content. While the intensity is extracted from the image, the curvature is introduced by the interpolation function. It has been empirically demonstrated that the use of the curvature, as incorporated into the information content of the Intensity-Curvature Functional, produces improvement of the interpolation error and should prove useful to determine improvement of estimation of signals at unknown locations. Starting from classic interpolation, it is thus possible to advance to a practical approach which uses the pixel intensity and the curvature of the interpolation function as combined and unique parameter to determine the novel SRE-based interpolation functions. Within this process it can be recognized that the concept that bridges classic interpolation to SRE-based interpolation is the curvature of the interpolator.

4.5 Numerical Example

To explain the meaning of the spatial set of points named Sub-pixel Efficacy Region, one needs to consider their effect on the interpolation function. Given a classic interpolation function, the values of the independent variable x are re-calculated within their domain of existence through the projection of the misplacement x_0 onto the novel re-sampling locations x^{r0}. Therefore, the effect of the Sub-pixel Efficacy Region is that the function is re-mapped versus a novel set of independent variables x^{r0}. This process is illustrated in Fig. 9a where the one-dimensional signal sin (x) is shown in the original form (black). It is then re-sampled through the quadratic B-Spline at a location $x_0 = 0.02$ ("a"=-2.87), and motion corrected of 0.02 by the B-Spline to obtain a RMSE = 0.0191. The resulting curve is shown by the black dashed line. Also, the signal is motion corrected of $x^{r0} \neq x_0$ by the SRE-based B-Spline, which is the classic (7) where it is used $x = x^{r0}$ but not $x = x_0$. The resulting signal is shown in white and the approximation is thus improved (RMSE = 0.0186). The value of x^{r0} is obtained from (12) and it is not necessarily the same for each of the intra-node

intervals. Consistently, figure 9b shows the misplacement $x_0 = 0.02$ (black), the SRE coordinate x_{sre} (dashed), and the novel re-sampling locations x^{r0} (white) in their evolution across the intra-node intervals [0.3, 2.9], for the given resolution of 0.1.

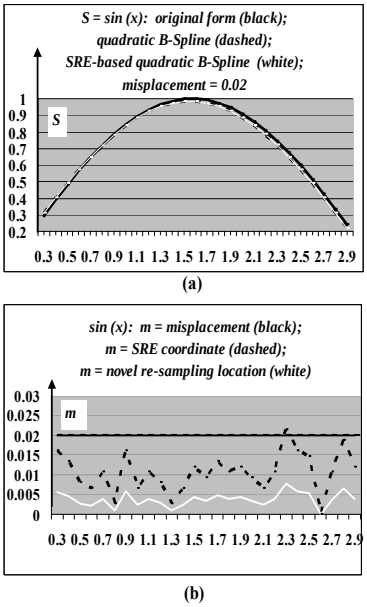

Figure 9. (a) One-dimensional signal sin (x) (black), re-sampled and motion corrected with classic B-Spline and SRE-based B-Spline, respectively and shown by the dashed black line and the white line. (b) Plot of the misplacement (black), of the x_{sre} coordinate (black dashed), and of the novel re-sampling locations x^{r0} (white), in their evolution across the intra-node intervals [0.3, 2.9].

4.6 Conclusion

The main contribution of the theory presented here is the mathematical characterization of a spatial domain called Sub-pixel Efficacy Region which is constituted by a set of intra-pixel points that, for given re-sampling location, allows calculating novel re-sampling locations where the interpolation error is improved. This is done within a unifying framework which groups together under the same methodological approach: trivariate linear and quadratic B-Spline interpolation functions. Thus, in this paper, the framework has determined novel schemes of these two functions with improved approximation capabilities, while reporting results previously obtained applying the theory to bivariate linear [18] and cubic Lagrange interpolation functions.

5. References

[1] S. P. Raya and J. K. Udupa. Shape-based Interpolation of Multidimensional Objects..IEEE Trans. Med. Imag., 9 (1): 32-42, 1990.

[2] G. T. Herman, J. Zheng, and A. Bucholtz. Shape-based Interpolation. IEEE Comp. Graph. & Applic., 12 (3): 69-79, 1992.

[3] G. J. Grevera, and J. K. Udupa. Shape-based Interpolation of Multidimensional Grey-Level Images. IEEE Trans. Med. Imag., 15 (6):,881-892, 1996.

[4] G. J. Grevera, and J. K. Udupa. An Objective Comparison of 3-D Image Interpolation Methods. IEEE Trans, Med. Imag., 17 (4): 642-652, 1998.

[5] W. E. Higgins, C. Morice, and E. L. Ritman. Shape-Based Interpolation of Tree-Like Structures in Three-Dimensional Images. IEEE Trans. Med. Imag., 12 (3): 439-450, 1993.

[6] G. P. Penney, J. A. Schnabel, D. Rueckert, M. A. Viergever, and W. J. Niessen. Registration-Based Interpolation. IEEE Trans. Med. Imag., 23 (7): 922-926, 2004.

[7] M. Unser, P. Thevenaz, and L. Yaroslavsky. Convolution-Based Interpolation for Fast, High-Quality Rotation of Images. IEEE Trans. Imag. Proc., 4 (10): 1371-1381, 1995.

[8] R. P. Agarwal and P. J. Y. Wong. Error Inequalities in Polynomial Interpolation and Their Applications. In: Mathematics and Its Applications, Kluwer Academic Publishers, The Netherlands, 1993.

[9] T. Blu, P. Thevenaz and M. Unser. MOMS: Maximal-Order Interpolation of Minimal Support. IEEE Trans. Imag. Proc., 10 (7): 1069-1080, 2001.

[10] M. Unser. Splines: A Perfect Fit for Signal and Image Processing. IEEE Sign Proc. Mag., 16: 22-38, 1999.

[11] G. Strang and G. Fix. A Fourier Analysis of the Finite Element Variational Method. In: Constructive Aspect of Functional Analysis, Cremonese, Rome, Italy, pp. 796-830, 1971.

[12] T. Blu, and M. Unser. Quantitative Fourier Analysis of Approximation Techniques: Part I – Interpolators and Projectors. IEEE Trans. Sign. Proc., 47 (10): 2783-2795, 1999.

[13] P. Thevenaz, T. Blu, and M. Unser. Interpolation Revisited. IEEE Trans. Med. Imag., 19 (7): 739-758, 2000.

[14] J. Wang. Optimal Design for Linear Interpolation of Curves. Statistics in Medicine, 20: 2467-2477, 2001.

[15] L. Joyeux and P. A. Penczeck. Efficiency of 2D Alignment Methods. Ultramicroscopy, 92: 33-46, 2002.

[16] X. Deng and T. S. Denney, Jr. On Optimizing Knot Positions for Multi-dimensional B-Spline Models. In: Proc. IS & T SPIE, 2004.

[17] R.L. Buckner, A.Z. Snyder, A.L. Sanders, M.E. Raichle, and J.C. Morris. Functional Brain Imaging of Young Non-Demented and Demented Older Adults. Journal of Cognitive Neuroscience, 12-2, 2000.

[18] C. Ciulla and F.P. Deek. On the Approximate Nature of the Bivariate Linear Interpolation Function: A Novel Scheme Based on Intensity-Curvature. ICGST - International Journal on Graphics, Vision and Image Processing, 5 (7): 9-19, 2005.

[19] T. M. Lehmann, C. Gonner, and K. Spitzer. Survey: Interpolation Methods in Medical Image Processing. IEEE Trans. Med. Imag., 18 (11): 1049-1075, 1999.

[20] T.M. Lehmann, C. Gonner, and K. Spitzer. Addendum: B-Spline Interpolation in Medical Image Processing. IEEE Trans. Med. Imag., 20 (7): 660-665, 2001.

[21] M. Unser. A. Aldroubi, and M. Eden. B-Spline Signal Processing: Part I – Theory. IEEE Trans. Sign. Proc., 41 (2): 821-833, 1993a.

[22] M. Unser. A. Aldroubi, and M. Eden. B-Spline Signal Processing: Part II – Efficient Design and

Applications. IEEE Trans. Sign. Proc., 41 (2): 834-847, 1993b.
[23] S. Samadi, M.O. Ahmad, and M.N.S. Swamy. Characterization of B-Spline Digital Filters. IEEE Trans. Circ. Syst., 51 (4): 808-816, 2004.
[24] C. de Boor. A practical Guide to Splines. In: Applied Mathematical Sciences, Springer-Verlag, New York, 1978.
[25] T. Blu, P. Thevenaz, and M. Unser. Complete Parameterization of Piecewise-polynomial Interpolation Kernels. IEEE Trans. Imag. Proc., 12 (11): 1297-1309, 2003.
[26] I. Newton and C. Huygens. Mathematical Principles of Natural Philosophy. R.M. Hutchins (Editor), pp. 338-339, William Benton, 1934.
[27] I. J. Schoenberg. Contribution to the Problem of Approximation of Equidistant Data by Analytic Functions. Part A – On the Problem of Smoothing and Graduation. A First Class of Analytic Approximation Formulaes. Quart. Appl. Math., 4 (1): 112-141, 1946.
[28] I. J. Schoenberg. Cardinal Interpolation and Spline Functions. J. Approx .Theory, 2 (2): 167-206, 1969.